Biomedical Optics EXPRESS

Non-invasive transdermal two-dimensional mapping of cutaneous oxygenation with a rapid-drying liquid bandage

Zongxi Li,[1] Emmanuel Roussakis,[1] Pieter G. L. Koolen,[2] Ahmed M. S. Ibrahim,[2] Kuylhee Kim,[2] Lloyd F. Rose,[3] Jesse Wu,[3] Alexander J. Nichols,[1,4,5] Yunjung Baek,[1, 6] Reginald Birngruber,[7] Gabriela Apiou-Sbirlea,[1] Robina Matyal,[8] Thomas Huang,[8] Rodney Chan,[3] Samuel J. Lin,[2] and Conor L. Evans[1,4,*]

[1]*Wellman Center for Photomedicine, Harvard Medical School, Massachusetts General Hospital, 149 13th Street, Charlestown, Massachusetts 02129, USA*

[2]*Division of Plastic Surgery, Harvard Medical School, Beth Israel Deaconess Medical Center, 110 Francis Street Suite 5A, Boston, Massachusetts 02215, USA*

[3]*Dental and Trauma Research Detachment, U.S. Army Institute of Surgical Research, 3698 Chambers Pass, Suite B, JBSA –Fort Sam Houston, Texas 78234-7767, USA*

[4]*Harvard University Program in Biophysics, Building C2 Room 112, 240 Longwood Avenue, Boston, MA 02115, USA*

[5]*Harvard-MIT Division of Health Sciences and Technology, 77 Massachusetts Avenue E25-519, Cambridge, MA 02139, USA*

[6]*Department of Chemistry, Korea Advanced Institute of Science and Technology (KAIST), 291 Daehak-ro, Yuseong-gu, Daejeon 305-701, South Korea*

[7]*University of Lübeck, Institute of Biomedical Optics, Lübeck, Peter Monnik Weg 4, 23562 Lübeck, Germany*

[8]*Department of Anesthesia, Critical Care and Pain Medicine, Harvard Medical School, Beth Israel Deaconess Medical Center, 330 Brookline Avenue, Boston, Massachusetts 02215, USA*

**evans.conor@mgh.harvard.edu*

Abstract: Oxygen plays an important role in wound healing, as it is essential to biological functions such as cell proliferation, immune responses and collagen synthesis. Poor oxygenation is directly associated with the development of chronic ischemic wounds, which affect more than 6 million people each year in the United States alone at an estimated cost of $25 billion. Knowledge of oxygenation status is also important in the management of burns and skin grafts, as well as in a wide range of skin conditions. Despite the importance of the clinical determination of tissue oxygenation, there is a lack of rapid, user-friendly and quantitative diagnostic tools that allow for non-disruptive, continuous monitoring of oxygen content across large areas of skin and wounds to guide care and therapeutic decisions. In this work, we describe a sensitive, colorimetric, oxygen-sensing paint-on bandage for two-dimensional mapping of tissue oxygenation in skin, burns, and skin grafts. By embedding both an oxygen-sensing porphyrin-dendrimer phosphor and a reference dye in a liquid bandage matrix, we have created a liquid bandage that can be painted onto the skin surface and dries into a thin film that adheres tightly to the skin or wound topology. When captured by a camera-based imaging device, the oxygen-dependent phosphorescence emission of the bandage can be used to quantify and map both the pO_2 and oxygen consumption of the underlying tissue. In this proof-of-principle study, we first demonstrate our system on a rat ischemic limb model to show its capabilities in sensing tissue ischemia. It is then tested on both *ex vivo* and *in vivo* porcine burn models to monitor the progression of burn injuries. Lastly, the bandage is applied to an *in vivo* porcine graft model for monitoring the integration of full- and partial-thickness skin grafts.

#217203 - $15.00 USD Received 22 Jul 2014; revised 5 Sep 2014; accepted 5 Sep 2014; published 1 Oct 2014

OCIS codes: (170.2655) Functional monitoring and imaging; (160.2540) Fluorescent and luminescent materials; (170.3880) Medical and biological imaging; (170.6510) Spectroscopy, tissue diagnostics.

References and links

1. C. K. Sen, "Wound healing essentials: let there be oxygen," Wound Repair Regen. **17**(1), 1–18 (2009).
2. A. Bishop, "Role of oxygen in wound healing," J. Wound Care **17**(9), 399–402 (2008).
3. C. K. Sen, G. M. Gordillo, S. Roy, R. Kirsner, L. Lambert, T. K. Hunt, F. Gottrup, G. C. Gurtner, and M. T. Longaker, "Human skin wounds: a major and snowballing threat to public health and the economy," Wound Repair Regen. **17**(6), 763–771 (2009).
4. M. Reddy, D. Keast, E. Fowler, and R. G. Sibbald, "Pain in pressure ulcers," Ostomy Wound Manage. **49**(4 Suppl), 30–35 (2003).
5. F. Gottrup, "Oxygen in wound healing and infection," World J. Surg. **28**(3), 312–315 (2004).
6. S. Schreml, R. M. Szeimies, L. Prantl, S. Karrer, M. Landthaler, and P. Babilas, "Oxygen in acute and chronic wound healing," Br. J. Dermatol. **163**(2), 257–268 (2010).
7. J. L. Burns, J. S. Mancoll, and L. G. Phillips, "Impairments to wound healing," Clin. Plast. Surg. **30**(1), 47–56 (2003).
8. D. Xing, L. Liu, G. P. Marti, X. Zhang, M. Reinblatt, S. M. Milner, and J. W. Harmon, "Hypoxia and hypoxia-inducible factor in the burn wound," Wound Repair Regen. **19**(2), 205–213 (2011).
9. S. T. Lee and A. M. Scott, "Hypoxia positron emission tomography imaging with 18f-fluoromisonidazole," Semin. Nucl. Med. **37**(6), 451–461 (2007).
10. G. H. Takahashi, I. Fatt, and T. K. Goldstick, "Oxygen consumption rate of tissue measured by a micropolarographic method," J. Gen. Physiol. **50**(2), 317–335 (1966).
11. C. Ruangsetakit, K. Chinsakchai, P. Mahawongkajit, C. Wongwanit, and P. Mutirangura, "Transcutaneous oxygen tension: a useful predictor of ulcer healing in critical limb ischaemia," J. Wound Care **19**(5), 202–206 (2010).
12. H. H. Moosa, M. S. Makaroun, A. B. Peitzman, D. L. Steed, and M. W. Webster, "TcPO2 Values in Limb Ischemia: Effects of Blood Flow and Arterial Oxygen Tension," J. Surg. Res. **40**(5), 482–487 (1986).
13. K. M. Baldwin, "Transcutaneous oximetry and skin surface temperature as objective measures of pressure ulcer risk," Adv. Skin Wound Care **14**(1), 26–31 (2001).
14. J. M. Vanderkooi, G. Maniara, T. J. Green, and D. F. Wilson, "An optical method for measurement of dioxygen concentration based upon quenching of phosphorescence," J. Biol. Chem. **262**(12), 5476–5482 (1987).
15. Y. Amao, "Probes and Polymers for Optical Sensing of Oxygen," Mikrochim. Acta **143**(1), 1–12 (2003).
16. S. M. Borisov, G. Zenkl, and I. Klimant, "Phosphorescent platinum(II) and palladium(II) complexes with azatetrabenzoporphyrins-new red laser diode-compatible indicators for optical oxygen sensing," ACS Appl. Mater. Interfaces **2**(2), 366–374 (2010).
17. C. S. Chu, Y. L. Lo, and T. W. Sung, "Enhanced oxygen sensing properties of Pt(II) complex and dye entrapped core-shell silica nanoparticles embedded in sol-gel matrix," Talanta **82**(3), 1044–1051 (2010).
18. M. B. Winter, E. J. McLaurin, S. Y. Reece, C. Olea, Jr., D. G. Nocera, and M. A. Marletta, "Ru-porphyrin protein scaffolds for sensing O_2," J. Am. Chem. Soc. **132**(16), 5582–5583 (2010).
19. C. Wu, B. Bull, K. Christensen, and J. McNeill, "Ratiometric single-nanoparticle oxygen sensors for biological imaging," Angew. Chem. Int. Ed. Engl. **48**(15), 2741–2745 (2009).
20. I. Dunphy, S. A. Vinogradov, and D. F. Wilson, "Oxyphor R2 and G2: phosphors for measuring oxygen by oxygen-dependent quenching of phosphorescence," Anal. Biochem. **310**(2), 191–198 (2002).
21. F. Niedermair, S. M. Borisov, G. Zenkl, O. T. Hofmann, H. Weber, R. Saf, and I. Klimant, "Tunable phosphorescent NIR oxygen indicators based on mixed benzo- and naphthoporphyrin complexes," Inorg. Chem. **49**(20), 9333–9342 (2010).
22. A. Y. Lebedev, A. V. Cheprakov, S. Sakadzić, D. A. Boas, D. F. Wilson, and S. A. Vinogradov, "Dendritic phosphorescent probes for oxygen imaging in biological systems," ACS Appl. Mater. Interfaces **1**(6), 1292–1304 (2009).
23. X. D. Wang, and O. S. Wolfbeis, "Optical methods for sensing and imaging oxygen materials, spectroscopies and applications," Chem. Soc. Rev. **43**(10), 3666–3761 (2014).
24. S. Schreml, R. J. Meier, O. S. Wolfbeis, T. Maisch, R. M. Szeimies, M. Landthaler, J. Regensburger, F. Santarelli, I. Klimant, and P. Babilas, "2D luminescence imaging of physiological wound oxygenation," Exp. Dermatol. **20**(7), 550–554 (2011).
25. A. Mahnke, R. J. Meier, V. Schatz, J. Hofmann, K. Castiglione, U. Schleicher, O. S. Wolfbeis, C. Bogdan, and J. Jantsch, "Hypoxia in Leishmania major Skin Lesions Impairs the NO-Dependent Leishmanicidal Activity of Macrophages," J. Invest. Dermatol. **134**(9), 2339–2346 (2014), doi:10.1038/jid.2014.121.
26. J. Hofmann, R. J. Meier, A. Mahnke, V. Schatz, F. Brackmann, R. Trollmann, C. Bogdan, G. Liebsch, X.-D. Wang, O. S. Wolfbeis, and J. Jantsch, "Ratiometric luminescence 2D in vivo imaging and monitoring of mouse skin oxygenation," Methods Appl. Fluoresc. **1**(4), 045002 (2013).
27. J. S. Boateng, K. H. Matthews, H. N. Stevens, and G. M. Eccleston, "Wound healing dressings and drug delivery systems: a review," J. Pharm. Sci. **97**(8), 2892–2923 (2008).
28. N. J. Turro, *Modern Molecular Photochemistry* (University Science Books, Sausalito, CA, 1991).

#217203 - $15.00 USD Received 22 Jul 2014; revised 5 Sep 2014; accepted 5 Sep 2014; published 1 Oct 2014

29. X. D. Wang, R. J. Meier, M. Link, and O. S. Wolfbeis, "Photographing oxygen distribution," Angew. Chem. Int. Ed. Engl. **49**(29), 4907–4909 (2010).
30. S. V. Apreleva, D. F. Wilson, and S. A. Vinogradov, "Tomographic imaging of oxygen by phosphorescence lifetime," Appl. Opt. **45**(33), 8547–8559 (2006).
31. S. A. Vinogradov, M. A. Fernandez-Seara, B. W. Dupan, and D. F. Wilson, "A method for measuring oxygen distributions in tissue using frequency domain phosphorometry," Comp. Biochem. Physiol. A Mol. Integr. Physiol. **132**(1), 147–152 (2002).
32. T. J. Kelechi and D. E. Neal, "Skin perfusion pressure in chronic venous disorders," Adv. Skin Wound Care **21**(12), 576–581 (2008).
33. E. Faglia, G. Clerici, M. Caminiti, A. Quarantiello, V. Curci, and F. Somalvico, "Evaluation of feasibility of ankle pressure and foot oximetry values for the detection of critical limb ischemia in diabetic patients," Vasc. Endovascular Surg. **44**(3), 184–189 (2010).
34. C. C. Powell, S. C. Schultz, D. G. Burris, W. R. Drucker, and D. S. Malcolm, "Subcutaneous oxygen tension: A useful adjunct in assessment of perfusion status," Crit. Care Med. **23**(5), 867–873 (1995).
35. G. S. E. Dowd, K. Linge, and G. Bentley, "Measurement of transcutaneous oxygen pressure in normal and ischemic skin," J. Bone Joint Surg. **65**(1), 79–83 (1983).
36. J. Barret-Nerin and D. N. Herndon, Principles and Practice of Burn Surgery (New York: Marcel Dekker, 2004).
37. A. Papp, K. Kiraly, M. Härmä, T. Lahtinen, A. Uusaro, and E. Alhava, "The progression of burn depth in experimental burns: a histological and methodological study," Burns **30**(7), 684–690 (2004).
38. A. Coruh and Y. Yontar, "Application of split-thickness dermal grafts in deep partial- and full-thickness burns: a new source of auto-skin grafting," J. Burn Care Res. **33**(3), e94–e100 (2012).
39. J. W. Alexander, B. G. MacMillan, E. Law, and D. S. Kittur, "Treatment of severe burns with widely meshed skin autograft and meshed skin allograft overlay," J. Trauma **21**(6), 433–438 (1981).

1. Introduction

Oxygen is essential for maintaining the viability of skin and its contents [1]. The ability to measure cutaneous oxygen status non-invasively is needed for the treatment of a variety of skin diseases including chronic and ischemic wounds, burn wounds and large, complex wounds that require skin replacement. Measuring tissue oxygen tension helps diagnose, prevent and monitor the therapeutic response of ischemic conditions. It also allows for the monitoring of flap/graft perfusion and aids in the early detection of flap/graft failure. Additionally, measuring the dynamic changes in pO_2 on the skin surface can provide information on the oxygen consumption properties of the underlying tissue, which can in turn help identify tissue that is metabolically deviated from normal.

Chronic wounds, largely resulting from ischemia, are prevalent conditions accounting for twenty percent of non-traumatic wounds, with an estimated $25 billion dollars in treatment cost per year [2, 3]. The prevalence of these wounds is linked directly to increased aging demographics, vascular disease, venous insufficiency, mechanical pressure and diabetic vasculopathy. Chronic wounds that develop due to tissue hypoxia are not only painful, but are the leading cause of prolonged hospitalization [4]. If not treated properly, infections and other complications may occur. In addition to its causative role in various skin conditions, the presence of tissue hypoxia also significantly worsens disease prognosis [1, 2, 5, 6]. Wound healing is highly oxygen-dependent due to the increased energy demand for tissue reparative processes such as cell proliferation, response to infections and collagen synthesis; damaged tissue deprived of adequate blood flow has a decreased ability to heal [1, 7].

The surgical therapy for burns is another example where objective measurements of cutaneous oxygenation may improve outcomes. Currently, the clinical determination of burn depth and therefore the decision for surgical debridement depends on subjective visual assessments, or rarely, invasive techniques such as a skin biopsy. Accurate determination of burn depth based on cutaneous oxygenation may decrease unnecessary surgery. The ability to determine tissue viability would also allow for the monitoring of skin graft and skin substitute integration in patients whom skin replacement is needed after burn debridement.

Many previous attempts have been made to develop technologies that allow the detection of tissue oxygenation. Histochemical staining with hypoxia markers such as pimonidazole provides semi-quantitative detection of tissue hypoxia, and radioactively labeled markers have been developed that can be imaged by positron emission tomography (PET) [8, 9].

#217203 - $15.00 USD Received 22 Jul 2014; revised 5 Sep 2014; accepted 5 Sep 2014; published 1 Oct 2014

However, this method requires the injection of exogenous markers and later either tissue biopsy, or specialized instrumentation to identify the markers. It is therefore labor-intensive and also may be limited by the spatial resolution of the PET scanners. The needle-type Clark electrodes can precisely measure pO_2 and are the gold standard for the clinical assessment of tissue oxygenation [1]. However, placing a needle electrode into tissue 1) is necessarily restricted to point measurements, 2) is invasive and can be painful, and 3) causes tissue injury that can alter microcirculation and thus the pO_2 levels being measured [10]. Although planar electrodes have been designed that allow the measurement of transcutaneous oxygen pressure (TcPO2) by attaching probes on the skin surface, these tools require heating the examined skin to 44-45 °C, beyond the average physiological temperature. Furthermore, TcPO2 devices only allow point measurements, making multiple measurements necessary for the assessment of the entire area under examination [11, 12].

Other non-invasive methods, such as pulse oximetry, estimate tissue oxygenation by calculating the ratio between oxygenated and deoxygenated hemoglobin using its oxygen-dependent spectral properties [13]. However, the results of this indirect approach do not necessarily represent absolute tissue oxygenation, since 1) they only provide the relative amount of oxy/deoxy hemoglobin (oxygen saturation) but not total oxygen supply, and 2) they provide no information about oxygen consumption rate. For example, an inflammatory area with normal oxygen saturation as measured in the blood vessels can still be hypoxic due to rapid oxygen consumption by the highly metabolic cells surrounding the blood vessel. Due to these crucial limitations, few studies exist on tissue oxygenation in acute wounds and fewer still on tissue oxygenation in chronic wounds [1]. These and other factors have created a long-standing need for a technology that allows rapid and non-invasive tissue oxygenation quantification across a wound site without cumbersome tools and that can be read easily without extensive training.

A sensitive approach to quantify tissue oxygenation utilizes a process known as oxygen-dependent quenching of phosphorescence [14]. Phosphorescence of a molecular sensor can be quenched by collision with oxygen, resulting in energy transfer from the excited triplet state of the phosphor to ground-state triplet oxygen molecules. As a result, the sensor's phosphorescence lifetime decreases and is inversely proportional to the concentration of oxygen present in the molecule's surroundings. Among the existing oxygen-sensing phosphors, metalloporphyrins have attracted much attention due to their unique photophysical properties, such as multiple excitation bands and relatively long-lived, room temperature phosphorescence in the red and near-infrared spectral region. Metalloporphyrin-based molecular sensors have been used to measure vascular oxygen tension in organs such as kidney, heart and brain in various animal models [15–22]. Creating a layer of film containing such phosphors for the monitoring of tissue oxygenation status has the advantage of providing a continuous, quantitative *two-dimensional map* of pO_2 in real time as opposed to the single point measurement obtained by the TcPO2 device, therefore allowing for a more rapid and comprehensive assessment of tissue perfusion. Such an approach would not, in principle, require any patient-specific calibration and could be carried out repeatedly under physiological conditions. Pioneering work in the development of such sensing films has been reported by Wolfbeis and his colleagues [23], including their use in visualizing wounds [24] and infections [25] via both lifetime measurements and measuring changes in phosphorescence intensity [26].

There is an unmet clinical need for the development of a breathable, transparent, simple-to-apply-and-read and easily removable bandage [27] for mapping oxygen across skin, burns, and grafts, that can report oxygen, protect the underlying tissue, and enable visual inspection of tissue through the bandage itself. In this report, we present a novel oxygen-sensing, rapid-drying paint-on bandage that can be applied to the surface of skin for two-dimensional tissue oxygenation mapping, designed for the monitoring of burns and tissue grafts. By embedding oxygen-sensing molecules within a transparent, polymeric liquid bandage material, the sensor

#217203 - $15.00 USD Received 22 Jul 2014; revised 5 Sep 2014; accepted 5 Sep 2014; published 1 Oct 2014

can be painted on the surface of the skin as a viscous liquid and allowed to dry against the wound topology to form a solid tight seal. To ensure facile oxygen sensing a porphyrin-dendrimer was utilized, where a metallated porphyrin as phosphorescent core was surrounded by a dendritic structure. The dendrimer not only reduced the collisional frequency of oxygen with the porphyrin core by attenuating oxygen diffusion through its branches, but also increased compatibility with the liquid bandage components, allowing for homogeneous distribution of the molecule throughout the bandage setting process. This strategy enabled the bandage to reach an optimum dynamic range for oxygen sensing throughout physiological pO_2 values, and minimized porphyrin-porphyrin interactions that could lead to a decrease in porphyrin emissivity caused by self-quenching. Once the sensor was applied to the skin, a transparent barrier film was placed on top of the sensing bandage to reduce, but not eliminate, ambient oxygen exchange. The phosphorescence emission of the sensing bandage was captured by a custom camera and used to generate a two-dimensional oxygen map of the underlying tissue, via either a ratiometric or a lifetime-based approach. To enable highly sensitive measurements of skin oxygenation, a delay-trigger mechanism was designed to suppress tissue autofluorescence. Moreover, by temporally integrating the oxygen consumption beneath the bandage, tissue viability could be inferred. After use, the bandage was easily removed without disrupting the underlying tissue. This bandage system was first validated using an *in vivo* rat model to sense tissue ischemia. It was then tested on porcine burn models *ex vivo* and *in vivo* to monitor burn progression. Lastly, it was applied to an *in vivo* porcine graft model to visualize the integration of full-thickness and partial-thickness skin grafts.

2. Materials and methods

2.1. Oxygen-sensing paint-on bandage and camera based readout system

The oxygen sensitive phosphor and reference dye used in creating the sensing bandage were Pd-meso-tetra-(4-carboxyphenyl)porphyrin-dendrimer (Oxyphor R2) (Oxygen Enterprises, Ltd., Philadelphia, PA) and Coumarin 500 (Exciton, Dayton, OH), respectively. The long-lifetime Oxyphor R2 was specifically selected so that its long-lived phosphorescence could be distinguished from tissue autofluorescence using inexpensive timing circuitry. To ensure the solubility of the porphyrin dendrimer as well as its effective mixing with the liquid bandage components in both liquid and dried form, the terminal carboxy groups of the Oxyphor R2 were reacted with ethanol to form ethyl esters. The paint-on bandage mixture was formulated by mixing ethanol solutions of the esterified Oxyphor R2 (4.2 mM) and Coumarin 500 (10 mM) with the New-Skin® liquid bandage (Prestige Brands, Tarrytown, NY) at a volumetric ratio of 2:1:10. The breathable transparent film dressing Tegaderm® (1622W, 3M, Saint Paul, MN) was used as the barrier layer covering the sensing bandage to reduce the oxygen exchange between the sensing bandage and room air (Fig. 1).

Two Thyristor® electronic flash units (285-HV, Vivitar, Edison, NJ) equipped with 400/70 nm bandpass filters were used to provide a brief pulse of blue excitation light for both the oxygen-sensing phosphor (λ_{ex} = 415 nm) and the reference dye (λ_{ex} = 392 nm). A NIR CMOS camera (DCC3240N, Thorlabs, Newton, NJ) equipped with a 60 mm macrolens (Nikon, Melville, NY) was used to collect the emitted light from the sensing bandage. The phosphorescence of Oxyphor R2 ($\lambda_{em,max}$ = 690 nm) was captured as the "red-channel" image by placing a 700/70 nm bandpass filter at the camera lens front. The reference dye, Coumarin 500 ($\lambda_{em,max}$ = 495 nm), was imaged with a 510/10 nm bandpass filter and served as the "green-channel". The flash onset and the opening of the camera shutter were temporally coordinated by a digital delay/pulse generator (Stanford Research System, Sunnyvale, CA), so that images could be taken at arbitrary time points after the flash was triggered. Image analysis routines were performed in Matlab to generate the two-dimensional oxygen maps.

#217203 - $15.00 USD Received 22 Jul 2014; revised 5 Sep 2014; accepted 5 Sep 2014; published 1 Oct 2014

2.2. System calibration using phosphorescence intensity and lifetime

The oxygen-sensing paint-on bandage was calibrated by placing a dried sensing film inside a quartz cuvette with oxygen partial pressure controlled by a gas mixing system. The oxygen content was adjusted step-wise from 160 mmHg to 0 mmHg, and monitored in real-time using a needle-based Clark electrode (Unisense, Aarhus, Denmark). The system was allowed to stabilize at each step for 5 min before images were taken. Each calibration curve was averaged across three independent measurements.

For intensity-based calibration, a ratiometric approach was used. One red-channel (800 μs delay) and one green-channel (0 μs delay) image were taken at each pO_2 level. Reference-controlled phosphorescence intensity was calculated as red-to-green intensity ratio between the two channels and the reciprocal of this ratio was plotted over oxygen tensions to generate the intensity calibration curve.

For lifetime-based calibration, a series of red-channel/phosphorescence images were taken with the delay times set between the flash and the camera exposure varying from 0 to 10 ms. The intensity over delay time plot was obtained at each pO_2, and the phosphorescence lifetime τ was extracted from the curve. The reciprocal of the lifetime τ was then plotted over oxygen tensions to generate the lifetime calibration curve.

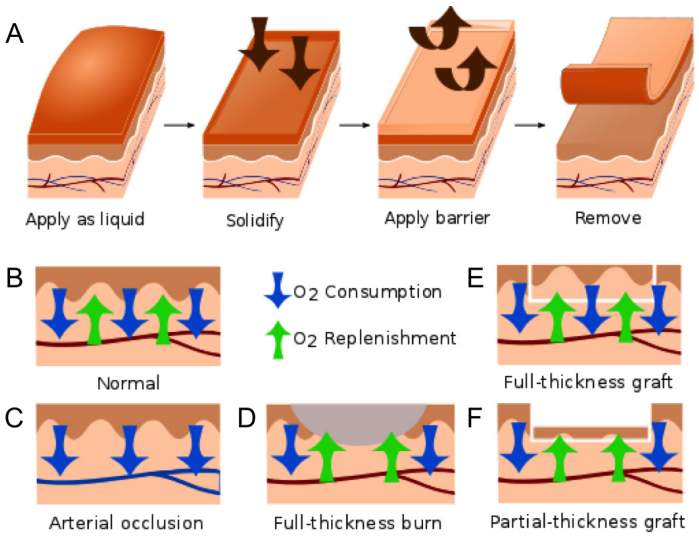

Fig. 1. A) Schematic diagram showing the application of the pO_2-sensing bandage as a liquid, bandage solidification, application of the barrier layer, and bandage removal after pO_2 measurement. The supply and consumption of oxygen in tissue balance to yield a measurable tissue oxygenation; B) balanced O_2 consumption and replenishment in normal skin; C) decreased surface pO_2 during tissue ischemia induced by arterial ligation; D) elevated surface pO_2 due to decreased O_2 consumption by necrotic tissue in a full-thickness burn; E) unaffected or slightly elevated surface pO_2 in a full-thickness skin graft; F) elevated surface pO_2 due to decreased O_2 consumption at a partial-thickness skin graft, which is composed of non-viable epithelial cells and only a thin layer (30/1000 inch) of dermal cells.

2.3. Sensing tissue ischemia in hindlimb using an in vivo rat model

Animal housing and maintenance: A total of eight Sprague-Dawley rats, weighing an average of 275 grams, were used. All rat procedures were performed within the Beth Israel Deaconess Medical Center animal facility. All members of the research team had completed the necessary CITI and LATA training modules for The Humane Care and Use of the Laboratory Rat, Aseptic Surgery of Rodents, Anesthesia and Analgesia of Rodents, Laboratory Rabbit, Laboratory Canine, and Laboratory Animals. The animal surgery protocol was reviewed and

#217203 - $15.00 USD Received 22 Jul 2014; revised 5 Sep 2014; accepted 5 Sep 2014; published 1 Oct 2014

approved by the Institutional Animal Care and Use Committee (IACUC) at the Beth Israel Deaconess Medical Center.

Anesthesia: The rats were placed into an induction chamber with 3% isoflurane in 100% oxygen at a flow rate of 1 L/min. When the rat was unresponsive to external stimuli, it was removed from the induction chamber and placed on a nose cone for maintenance of anesthesia. General anesthesia was maintained by administering 2% isoflurane at a 1 L/min flow rate.

Vessel exposure and occlusion: After inducing a complete state of anesthesia, the abdomen, thigh and ventral side of the animal's hind limb were shaved and aseptically prepared for surgery. Rats were positioned on their back and fixed in an X-shape using tape. A linear skin incision of 3 cm was made at the *linea alba* to expose the abdominal cavity. After cautious retraction of intra-abdominal organs, the retroperitoneal cavity was opened to ensure an optimal exposure of the descending aorta. Normal transdermal pO_2 was first measured on the left hind limb as a control (obtained under normal perfusion). A Clark electrode (Unisense, Aarhus, Denmark) was inserted into the gastrocnemius muscles of the hind limb of the rats to monitor the real-time in-tissue oxygen tension. The sensing bandage was painted onto the shaved skin above the region monitored by the electrode. The bandage was allowed to dry in air for 1 minute, and the barrier layer was applied. Equilibrium red- and green-channel images were captured after 15 min at 800 μs and 0 μs delay, respectively. After collecting images on the control leg, hindlimb ischemia was induced by clamping the animal's descending aorta with surgical micro vessel clips. The sensing bandage was then applied to the right hind limb and the imaging procedures were repeated to measure the transdermal pO_2 under ischemic conditions. Tissue pO_2 imaged were generated by calculating the intensity ratio between the red- and green-channel images and calibrated to the intensity calibration curve described in section 2.2.

Euthanasia: The rats were euthanized while under anesthesia by opening the diaphragm to elicit iatrogenic pneumothorax. They were then placed in a euthanasia chamber and 100% carbon dioxide was introduced. A fill rate of 10% to 30% of the chamber volume per minute with carbon dioxide (added to the existing air in the chamber) was used to achieve a balanced gas mixture and induce rapid unconsciousness with minimal distress to the animals. Death was confirmed by noting the animal's fixed and dilated pupils.

2.4. Measuring burn wound oxygenation on porcine skin explants

Full-thickness burns were created on freshly excised porcine skin *ex vivo* by bringing a brass rod, heated to 150°C, in contact with the surface of the skin for 15 seconds. Burn tissue damage was confirmed by histological analysis using hematoxylin and eosin staining. The oxygen-sensing bandage was applied 1 hour after the burn had been created, and allowed 1 min to dry in air. The bandage was also applied to an unburned skin sample that served as a control. The barrier layer was applied, and red- and green-channel images were taken both immediately and after 15 minutes of equilibration.

Tissue oxygenation in the *ex vivo* burn models was quantified based on phosphorescence intensity or lifetime. For intensity-based measurements, an 800 μs camera delay time was used while capturing the red-channel image to completely eliminate the skin autofluorescence background. The intensity of the red-channel image was divided by the intensity of its co-registered green-channel image and reconstructed into a ratiometric image using Matlab. 2-D tissue oxygenation maps were then obtained by correlating the intensity of the ratiometric image with pO_2 values at each image pixel, using the intensity calibration curve described in section 2.2. For lifetime-based measurements, three points on each decay curve were used for curve fitting to extract the phosphorescence lifetime τ. The lifetime at each image pixel was then correlated to pO_2 using the lifetime calibration curve described in section 2.2 to construct the 2-D tissue oxygenation map.

#217203 - $15.00 USD Received 22 Jul 2014; revised 5 Sep 2014; accepted 5 Sep 2014; published 1 Oct 2014

2.5. Monitoring wound progression of in vivo porcine full-thickness burns

Animal housing and maintenance: A Yorkshire cross-bred female pig (Midwest Research Swine, Gibbon, MN) aged 6 months and weighing 40-50 kg was used. This study was reviewed and approved by the Institutional Animal Care and Use Committee (IACUC) at the United States Army Institute of Surgical Research (USAISR, JBSA Fort Sam Houston, TX). All animals received care in strict compliance with the 2011 *Guide for the Care and Use of Laboratory Animals* by the National Research Council and were maintained in a facility accredited by the Association for Assessment and Accreditation of Laboratory Animal Care International (AAALAC, Int.).

Anesthesia, pre- and post-operative care: Pigs were anesthetized with Telazol® 6 mg/kg, intubated and maintained on isoflurane throughout the procedure. A 100 mcg Fentanyl patch was applied to the right ear for pain management. Prior to completion of the procedure, 4 mg hydromorphone was given intramuscularly for 6-8 hours of pain management. Following procedures, wound dressings, consisting of antibiotic-impregnated petrolatum (Xeroform) and cotton gauze, were secured to the wound beds for 7 days with Ioban. The dressing was removed at day 7 post operation. For follow-up observations, pigs were sedated with ketamine 10 mg/kg and maintained on isoflurane.

Burn creation: Five 6-cm wounds were marked (4 cm from each other and 2 cm from the spine) on each dorsal side of the animal and edges were tattooed. To create full-thickness burn, a brass cylinder (6 cm diameter) heated to 100°C was applied to the tattooed circles for 30 seconds. The total wound area accounted for less than 10% total body surface area (TBSA). The animal was allowed to recover for 7 days during which time a burn eschar developed.

For oxygen assessment, the sensing bandage was painted across the boundary of a burn wound. The camera was positioned so that the field of view spanned across a region that included both the tissue directly affected by the burn injury and the adjacent unburned skin. The barrier layer was applied and the bandage was allowed to equilibrate for 15 min. A green-channel image of the reference dye was captured with the 510/10 nm filter. The red-channel image was captured using the 700/70 nm filter with the camera delay time set to 800 μs to eliminate the skin autofluorescence background. Ratiometric images were constructed by plotting the intensity ratio between the red- and green-channel images, and a tissue oxygenation map was obtained by applying the intensity calibration to the ratiometric image. A follow-up assessment 7 days post-burn was performed to monitor the progression of the burn injury.

2.6. Monitoring integration of full-thickness and partial thickness skin grafts using in vivo porcine graft models

Animal housing and maintenance: The animal used in this experiment, the housing and maintenance procedures were the same as described in section 2.5.

Anesthesia, pre- and post-operative care: Pigs were anesthetized with Telazol® 6 mg/kg, intubated and maintained on isoflurane throughout the procedure. The back of the pig was sterilized by prepping with povidone-iodine solution and sterile surgical field was maintained throughout the procedure. Following suturing of the skin graft, wound dressings consisting of a bolster containing antibiotic-impregnated petrolatum (Xeroform) and cotton gauze were secured to the wound bed for 7 days. Additional protective dressing consisting of Ioban and cloth jacket were applied. The dressing was removed 7 days post operation.

Excision and grafting: Five 6-cm wounds were marked (4 cm from each other and 2 cm from the spine) on each dorsal side of the animal and edges were tattooed. Total wound area was less than 10% total body surface area. After full-thickness excision down to muscle fascia, wounds were covered with split-thickness autologous skin from a hindlimb donor site. Autografts of 30/1000th of an inch thickness were harvested using a Zimmer pneumatic

#217203 - $15.00 USD Received 22 Jul 2014; revised 5 Sep 2014; accepted 5 Sep 2014; published 1 Oct 2014

dermatome (Zimmer Surgical, Inc., Dover, OH) and cut to fit the defects. Full-thickness autograft skin was harvested from the original full-thickness wound creation and defatted surgically.

Tissue oxygenation in the full-thickness and partial-thickness skin grafts was assessed both immediately post grafting, as well as at 1-month follow up. The sensing bandage was painted across the boundary of the graft, and the camera was positioned so that the field of view spanned across a region that included both the graft and the skin immediately surrounding it. The barrier layer was applied and the bandage was allowed to equilibrate for 15 min. As above, a green-channel image of the reference dye was captured with the 510/10 nm filter. The red-channel image was captured using the 700/70 nm filter with the camera delay time set to 800 μs to eliminate the skin auto-fluorescence background. Ratiometric images were constructed by plotting the intensity ratio between the red- and green-channel images, and tissue oxygenation map was obtained by applying intensity calibration to the ratiometric image.

3. Results and discussion

3.1. Quantifying oxygen with ratiometric phosphorescence imaging and tissue auto-fluorescence background removal

The emission intensity and lifetime of a phosphorescent molecule can be used to quantify the O_2 content in the molecule's environment based on an oxygen-dependent quenching process. Molecular oxygen interacts with the excited triplet state of the phosphor through collisions, leading to the exchange of energy resulting in the phosphor's non-radiative decay to its ground state. Therefore both the phosphorescence intensity and lifetime decrease as a result of increasing oxygen content in the environment. The relationship between phosphorescence intensity/lifetime and pO_2 is described by the Stern-Volmer equation [28]:

$$I_0 / I = \tau_0 / \tau = 1 + K_{SV}[O_2] \ , \qquad (1)$$

where I and τ are the phosphorescence intensity and lifetime, respectively, at the measured oxygen concentration $[O_2]$; I_0 and τ_0 are the same measurements in the absence of oxygen; and K_{SV} is the Stern-Volmer quenching constant. While constructing the imaging device for the oxygen-sensing bandage, a 700/70 nm bandpass filter was chosen to capture the phosphorescence emission of the oxygen-sensing Oxyphor R2 molecule (λ_{em} = 690 nm). The quantification of pO_2 has been achieved on this camera-based imaging device using either phosphorescence intensity or lifetime measurement. The intensity-based approach is described here, and the lifetime approach will be discussed in detail in section 3.2.

Ratiometric approaches take advantage of the presence of an additional fluorophore in the bandage that provides an oxygen-independent signal as a reference and internal, built-in control [29]. In the case of the paint-on-bandage described in this work, phosphors and fluorophores are evenly distributed throughout the bandage formulation, such that the phosphorescence/fluorescence ratio is self-calibrated for any variation in bandage thickness over the tissue surface. All phosphorescence measurements recorded in the "red-channel" image were accompanied by a corresponding "green-channel" image of the Coumarin 500 reference dye. The red-to-green intensity ratio was calibrated to oxygen partial pressure.

Skin tissue is known to have strong autofluorescence that can interfere with the measurement of comparatively weak phosphorescence emission from the oxygen-sensing bandage. To actively suppress the short-lived tissue autofluorescence and extract only the longer-lifetime phosphorescence signal of interest, a delay-trigger mechanism was introduced. By opening the camera shutter several hundred microseconds after the flash, fluorescence emission from the skin is temporally gated out, and the long-lived phosphorescence emission can be selectively captured. The maximum phosphorescence-to-autofluorescence signal for the Oxyphor-containing bandage and imaging system was found

#217203 - $15.00 USD Received 22 Jul 2014; revised 5 Sep 2014; accepted 5 Sep 2014; published 1 Oct 2014

to occur at a delay of 800 μs. By using this approach, the delay-triggered camera exposure effectively eliminated the tissue autofluorescence background, and significantly increased the system's signal-to-noise ratio. The O_2 sensing calibration curve obtained using this intensity approach is shown in Fig. 2(A).

3.2. Phosphorescence lifetime imaging using a delay-triggered camera

As a means of quantifying oxygen, the phosphorescence lifetime signal is advantageous in that it is independent of any variation in excitation intensities or the amount of phosphor present in an imaged region [30]. Unfortunately, instruments for carrying out lifetime imaging often involve advanced light sources and high-speed detectors that can be expensive and cumbersome to use [31]. Typically, a short (generally nanosecond or shorter) excitation pulse is delivered to a phosphorescent sample, and the photon counts incident upon a detector are measured in a series of discretized time "bins," which group photon counts according to their arrival time at the detector. For a more straightforward and cost effective approach to obtaining two-dimensional maps of phosphorescence lifetime from the paint-on bandage, we utilized regular flash units as light source coupled with the delay-trigger system described above, alongside a mathematical model of phosphorescence decay. The flash units chosen for this study could be operated across a range of power settings, which was found to be highly advantageous.

Setting the flash units for lower power operation engages built-in circuitry that acts to rapidly quench light emission once the lamps reach a predetermined level, creating a burst of light similar to a square-wave shaped pulse. This enabled the blue excitation light provided by the flash units to be approximated as a square-wave pulse with 500 μs duration (Fig. 2). The phosphorescence decay of sensor molecules inside the bandage is convolved with this excitation pulse. This convolved decay curve can be generated by taking phosphorescence images of the bandage with a series of delay times set between the flash triggering time and the camera exposure. Then a deconvolution algorithm can be applied to this instrument measured decay curve to extract the lifetime of phosphorescence.

To achieve this, a theoretical model was created to describe the instrument-measured decay curve. Assuming the flash pulse is a square wave $P(t)$ with duration of τ_F, the phosphorescence emission by individual phosphor molecules decays over time following:

$$I(t) = I_0 e^{-t/\tau_P} \quad , \tag{2}$$

where I_0 and $I(t)$ are the phosphorescence intensity at time zero and time t, respectively, and τ_P is the phosphorescence lifetime of the sensor molecule. The phosphorescence signal convolved with the excitation pulse:

$$I_C(t) = (I * P)(t) = \int_0^t I(t-x)P(x)dx \tag{3}$$

which is a two-segment curve as shown in Fig. 2(B). Since the camera exposure time is much longer (15 ms) compared to the duration of the excitation pulse and the phosphorescence emission, the camera effectively integrates all incident phosphorescence intensity after the trigger time point. The brightness of the image captured by the camera as a function of the camera delay time is also a two-segment curve. For camera delay greater than the flash duration, it follows an exponential decay:

$$B(D) = \int_0^\infty I_C(t)dt = N\tau_P^2 I_0 (e^{\tau_F/\tau_P} - 1)e^{-D/\tau_P}, D > \tau_F \tag{4}$$

where B is the brightness of the camera captured image and D is the delay time set between the onset of flash excitation and camera exposure, N is the number of emissions triggered per unit time of exposure to the flash pulse (s^{-1}) and τ_F is the flash pulse duration (s). Using this

#217203 - $15.00 USD Received 22 Jul 2014; revised 5 Sep 2014; accepted 5 Sep 2014; published 1 Oct 2014

model, the theoretical intensity-delay curve can be plotted by inserting the measured flash duration (500 μs) and the unquenched phosphorescence lifetime of the Oxyphor R2 (700 μs) found in the literature [20]. The calculated decay curve matches very well with the experimental curve measured under zero oxygen partial pressure as shown in Fig. 2(D), validating the model as an accurate description of the system.

It should be noted from Eq. (4) that for delay time D greater than the flash duration τ_F, the curve follows an exponential decay with a rate constant equal to the phosphorescence lifetime of the sensor molecules. The unquenched phosphorescence lifetime of Oxyphor R2 extracted from the acquired decay curve was measured to be 692 ± 20 μs, which closely matches the reported lifetime of the molecule under similar conditions (701 ± 12 μs) [20]. Using this approach, the phosphorescence lifetime of the molecules inside the sensing bandage under different oxygen partial pressures was obtained from the experimentally measured intensity-delay curves under each pO_2 condition; in this manner, a lifetime calibration curve was generated for the system.

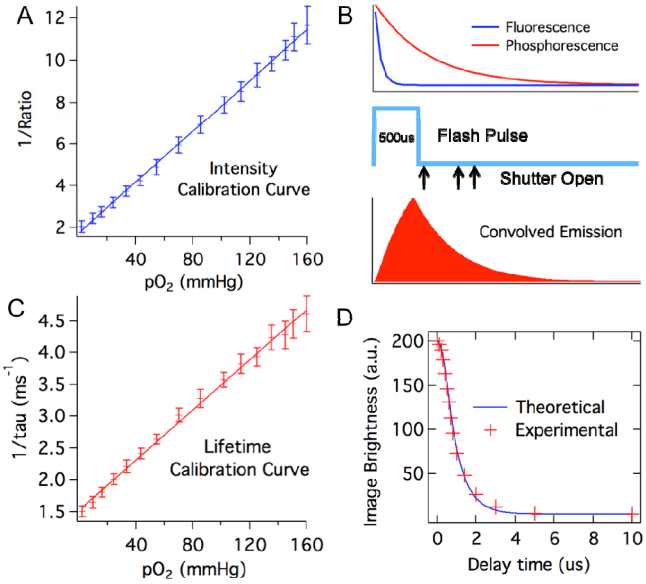

Fig. 2. Calibrating the oxygen-sensing bandage. A) System calibration curve based on phosphorescence intensity. Phosphorescent intensity is expressed as red-to-green channel intensity ratio. B) Timing events during the imaging process, showing the 500 μs illumination flash pulse relative to the phosphorescence decay of the oxygen sensor and the fluorescence decay of the reference dye; the camera shutter opens after predetermined delay times following the flash pulse; and phosphorescence emission convolved with the flash pulse. C) System calibration curve based on phosphorescence lifetime. D) Comparison between calculated and experimentally measured image brightness at camera delay time between 0 and 10 ms for Oxyphor R2-containing bandage under 0 mmHg pO_2. Calculation of image brightness was based on the assumption that the flash pulse is a square pulse with 500 μs pulse duration, and the phosphorescence lifetime of Oxyphor R2 under 0 mmHg pO_2 is 700 μs.

3.3. Sensing tissue ischemia in rats during arterial ligation

In a first validation experiment, the oxygen-sensing bandage was used to directly measure transdermal oxygenation through intact skin, where the equilibrium oxygen partial pressure reported by the bandage reflects the perfusion status of the underlying tissue. This application is of clinical relevance in the early detection of ischemic conditions, as shown in Fig. 1(C), and can be applied to monitor tissue ischemia at the engraftment sites on patients following graft, flap or other reconstructive surgeries for the early detection of graft/flap failure due to poor tissue perfusion. It can also be used to monitor other ischemic conditions such as

#217203 - $15.00 USD Received 22 Jul 2014; revised 5 Sep 2014; accepted 5 Sep 2014; published 1 Oct 2014

recurrent decubitus and diabetic ulcers, where tissue oxygenation plays a critical role in determining whether an ulcer will remain unhealed [2, 32, 33].

To demonstrate the oxygen-sensing bandage's ability to report tissue oxygenation *in vivo*, the bandage was applied to the hind limbs of eight rats where tissue ischemia was induced by arterial ligation. The average baseline intramuscular pO_2 in the rat's hindlimb recorded by a needle-based Clark electrode was 70 mmHg. The oxygen-sensing bandage was painted onto the skin of the rat's hindlimb directly above the region monitored by the Clark electrode. A two-dimensional map of transdermal pO_2 measured by the oxygen-sensing bandage under normal conditions is shown in Fig. 3. Under normal perfusion, the average transdermal pO_2 measured was 91.3 mmHg. When the descending aorta of the rats was surgically ligated, the intramuscular pO_2 measured by the Clark electrode decreased to 25 mmHg within 3 minutes and maintained between 20 and 30 mmHg throughout the duration of the ligation. This ischemia leads to a concomitant decrease in the observed transdermal pO_2. The average transdermal pO_2 under ischemia after 15 min of vessel ligation recorded by the oxygen-sensing bandage is 51.9 mmHg.

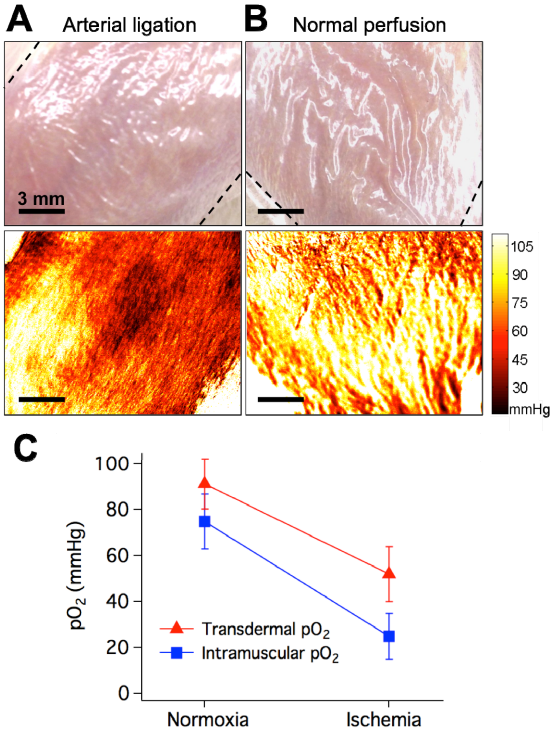

Fig. 3. Sensing tissue ischemia in the rat hindlimb. Red indicates lower tissue oxygenation and yellow indicates higher tissue oxygenation. Dashed lines indicate boundaries of bandage-covered region. A) Photograph (top) and tissue oxygenation map (bottom) taken during arterial ligation (lower tissue oxygenation). B) Photograph (top) and tissue oxygenation map (bottom) taken under normal perfusion (higher tissue oxygenation). C) Transdermal pO_2 measured by the sensing bandage and intramuscular pO_2 measured by the Clark electrode during normal perfusion and ischemia induced by arterial ligation.

The results measured by both methods were summarized in Fig. 3(C). The subcutaneous pO_2 measured by the Clark electrode under normoxic and ischemic conditions were consistent with the values measured by polarographic electrodes and TcPO2 devices reported in the literature [34, 35]. However, the transdermal pO_2 reported by the oxygen-sensing bandage was consistently higher than that measured with Clark electrode. This is expected because the

#217203 - $15.00 USD Received 22 Jul 2014; revised 5 Sep 2014; accepted 5 Sep 2014; published 1 Oct 2014

surface of skin is partially oxygenated by room air through diffusion through porous structures [1]. Also, as the bandage is calibrated to report absolute oxygen levels, the oxygen levels observed reflect the real oxygen concentration experienced by the bandage at any given time. This level may be higher than those measured by the Clark electrode as the bandage's barrier layer is breathable, such that the bandage experiences a mixture of both tissue and room oxygen levels. This choice of barrier layer was specifically made to ensure that tissue beneath the bandage receives adequate oxygenation. This difference in measurement can be compensated for by calibrating the bandage specifically for tissue applications, such as reporting oxygen levels for deep tissue structures. It should also be noted that this does not affect the bandage's ability to sense tissue hypoxia, as can be seen on Fig. 3(C) that the decrease in tissue oxygenation induced by arterial ligation was clearly reflected by the bandage measured transdermal pO_2.

3.4. Visualizing burns in porcine skin explants based on reduced oxygen consumption of necrotic tissues

In addition to the direct measurement of tissue oxygenation, the oxygen-sensing bandage can also be used to quantify average oxygen consumption rates by measuring the difference between initial and equilibrium pO_2 after applying the barrier layer. Given that all living, healthy tissues consume oxygen, this provides a tissue "vitality" map, and is especially useful in detecting tissue that is metabolically compromised (e.g. necrotic tissue in burns). It can potentially serve as a guide during burn debridement as well as in monitoring flap/graft viability in patients.

Acute and preoperative burns are characterized by the presence of a necrotic tissue layer [36], within which protein components of the dermis are coagulated along with dead cells. Surrounding this damaged tissue is a region characterized by reduced perfusion, where both cell viability and metabolism can be greatly compromised. Thus, when monitored transdermally, the oxygen consumption rate of tissue located at a burn wound is lower compared to healthy skin regions, as shown in Fig. 1(D). During standard-of-care debridement surgeries, it is not always possible to definitively determine where the necrotic zone ends and the zone of decreased perfusion begins. A technique based on measurement of tissue oxygen tension can allow the mapping of transdermal oxygen consumption rates for rapid visual identification of necrotic tissue within burn wound beds, potentially enhancing surgical efficacy and work flow.

To test the oxygen-sensing bandage's ability to visualize necrotic tissue in burns via oxygen consumption mapping, the bandage was first tested *ex vivo*. Full-thickness circular burns were created on freshly excised (still viable) porcine skin, and the oxygen-sensing bandage was painted over the burn as well as the surrounding skin area. Phosphorescence emission from the sensing bandage was first taken immediately after the application of the Tegaderm barrier layer to capture the initial pO_2 at the measurement site. After 15 minutes, images were taken again to capture the final oxygen partial pressure in the bandage environment after the bandage was given time to equilibrate with the underlying tissue. Percent tissue oxygen consumption rate (%) at each image pixel was calculated by taking the difference between the initial and equilibrium pO_2, and normalizing this value as a percentage of the maximum consumption measured in healthy skin.

The two-dimensional oxygen maps of burn wounds and control healthy skin were obtained using both intensity- and lifetime-based approaches and the results obtained are compared in Fig. 4. In the oxygen map generated using the ratiometric intensity-based approach, the circular burn region at the center of the skin sample can be seen to have a lower phosphorescence ratio compared to the surrounding skin area, which corresponds to higher equilibrium oxygen partial pressure, and thus lower oxygen consumption. This is consistent with the lower O_2 consumption rate of necrotic tissue. This is in clear contrast to the healthy control skin, where the equilibrium oxygen was low across the bandage-covered region. In

#217203 - $15.00 USD Received 22 Jul 2014; revised 5 Sep 2014; accepted 5 Sep 2014; published 1 Oct 2014

the lifetime-based image of the burn sample, the circular burn region demonstrated shorter phosphorescence lifetime of the bandage sensor, which also corresponds to higher oxygen partial pressure and lower oxygen consumption in the region.

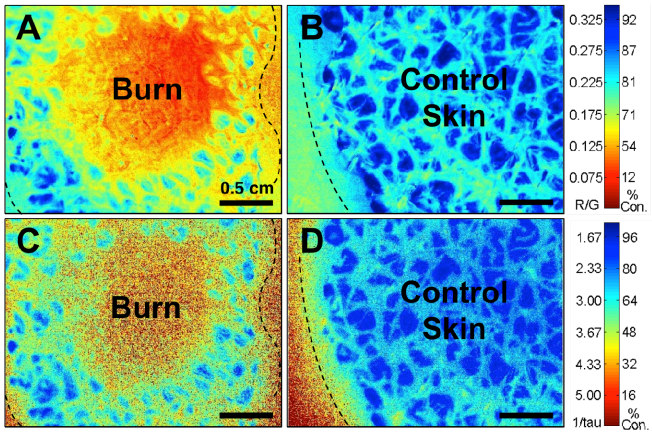

Fig. 4. Equilibrium oxygen maps showing a decrease of tissue oxygen consumption (expressed as normalized % consumption) by compromised tissue on freshly excised porcine skin obtained using intensity- and lifetime-based measurement approaches. Blue indicates higher oxygen consumption by tissues. Red indicates lower oxygen consumption (provides a visual "warning" for physiologically compromised tissue in clinical applications). Dashed line indicates boundaries of bandage-covered region. Images shown for A) Circular burn imaged using intensity approach; B) Control skin imaged using intensity approach; C) Circular burn imaged using lifetime approach; D) Control skin imaged using lifetime approach.

When comparing the images obtained using the intensity- and lifetime-approach, it can be noticed that the oxygen consumption rates measured by the two methods show similar patterns across the surface of the samples. The oxygen consumption values obtained using the intensity- and lifetime-calibration curves also correlate well with each other. It should be noted that it is easier to distinguish bandage-covered regions from bare skin on the lifetime-based images. This is because the signal generated from uncovered, bare skin contains only short-lived autofluorescence signal, the lifetime of which is significantly different from that of the phosphorescence emission from the bandage. It is also worthwhile to note that in comparing the images of the burn wound, the image of the burn region generated by the lifetime approach contains more noise. This is the direct result of the higher intrinsic error associated with high-oxygen tension lifetime measurements: when pO_2 values are high, the lifetime of the sensor molecule becomes much shorter and closer to zero. As the lifetime pO_2 decreases, it approaches the intrinsic noise of the imaging system and is more challenging to accurately measure.

As the surface of skin is not perfectly flat, surface roughness and tissue curvature can effect measurements in three ways. First, the natural curvature of the skin can, in some cases, cause only portions of tissue to lie within the camera's focal plane. While this may be challenging in future applications, the images taken in this study were acquired from relatively small, flat regions of skin such that the imaged tissue fell within the depth-of-field of the camera lens. Secondly, since the bandage is applied to the skin as a liquid, it coats the skin according to its surface topography, which means that the thickness of the bandage can vary with the small ridges and grooves of the skin. This effect is not expected to interfere with oxygen measurements, since the use of a reference dye effectively controls for the uneven distribution of bandage thickness, and lifetime measurements will not be effected by bandage thickness. Under certain conditions, surface roughness can lead to uneven attachment of the barrier layer. Small air pockets may form between the barrier layer and the natural grooves in the skin, which would, in turn, affect the oxygen equilibration process between the bandage

#217203 - $15.00 USD Received 22 Jul 2014; revised 5 Sep 2014; accepted 5 Sep 2014; published 1 Oct 2014

and the underlying tissue. When present, these air bubbles would lead to the measurement of oxygen consumption at values slightly lower than the rest of the skin.

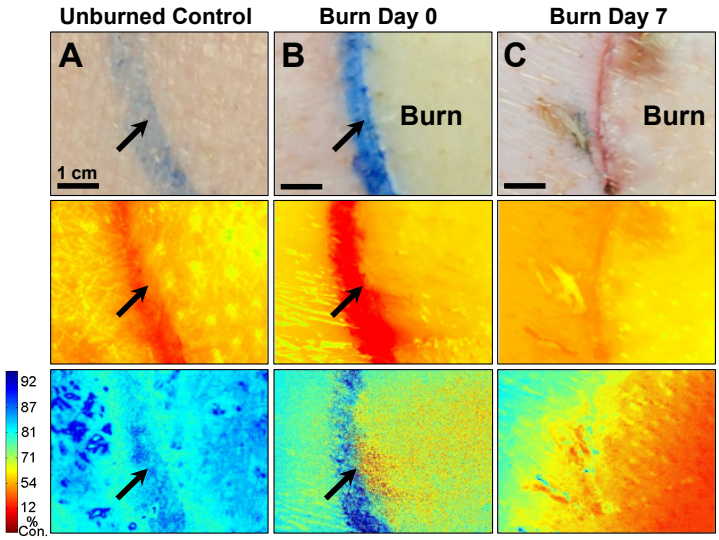

Fig. 5. Progression of a full-thickness burn on the paraspinal skin of a Yorkshire pig monitored by oxygen-sensing paint-on bandage. Images shown for A) control skin; B) immediately post-burn and C) 7 days post-burn. Top row: regular photographs; middle row: emission at 700 nm - oxygen-dependent phosphorescence signals are overwhelmed by the skin autofluorescence background; bottom-row: percent oxygen consumption (%) maps obtained after eliminating autofluorescence - blue indicates higher oxygen consumption by tissues. Red indicates lower oxygen consumption by tissues. Arrows indicate ink marks dividing burn and surrounding skin.

3.5. Monitoring in vivo burn wound progression using oxygen-sensing bandage in a porcine full-thickness burn model

Following testing with porcine explants, the next set of experiments focused on the bandage's ability to monitor burn wounds *in vivo*. Full-thickness circular burns were established on the paraspinal skin of a Yorkshire pig. Burn wound oxygenation was measured with the oxygen-sensing bandage both immediately after the creation of the burn and 7 days post-insult. Normal color photographs of the burn and control regions are shown in the top panel of Fig. 5. The middle panel shows the bandage emission captured at 700 nm without the delay exposure setting; therefore these images contain significant skin autofluorescence background. The bottom panels show the ratiometric intensity-based oxygen maps captured by the camera, where the autofluorescence background is eliminated by introducing the delay exposure mechanism. The early stages of tissue necrosis can be observed immediately after the creation of the burn as a region with elevated equilibrium pO_2. Progression of the burn injuries was observed during the 7-day follow-up assessment. A higher deviation from normal oxygen consumption rate was found, which correlated with an increased severity of tissue necrosis. Importantly, the oxygen-sensing bandage revealed that the area of necrosis had extended beyond the original burn region, an observation not easily made from the color photograph.

These results match the physiological changes known to occur following burn injuries. The local response to burn gives rise to three distinct tissue zones: the zone of coagulation refers to the central necrotic region featuring irreversible tissue loss; the surrounding zone of stasis is potentially salvageable, but can convert into complete tissue loss if the perfusion is poor; the outermost zone of hyperemia features increased perfusion as a response to the insult. In the photograph of the burn wound taken immediately following the injury, the

#217203 - $15.00 USD Received 22 Jul 2014; revised 5 Sep 2014; accepted 5 Sep 2014; published 1 Oct 2014

region inside the tattoo line shows apparent changes in tissue color (blanching), which marks irreversible cell necrosis. The O_2 consumption map shows a corresponding decrease of pO_2 consumption in the necrotic region, and also a slight elevation of pO_2 in the region immediately outside the tattoo line. This regional elevation can likely be attributed to increased perfusion corresponding to the zone of hyperemia. In the O_2 consumption map obtained during the 7-day follow-up, the region inside the tattoo showed greater deviation from normal tissue consumption, which can be explained by a deepening of the wound. The area immediately surrounding the original burned region also showed significant deviation from normal consumption, which is to be linked to wound progression and widening from additional tissue loss [37].

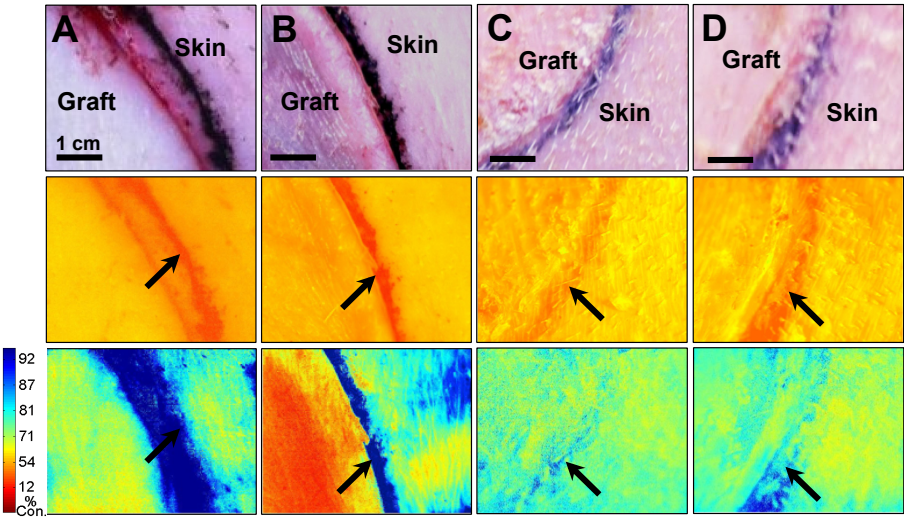

Fig. 6. Incorporation of full-thickness and partial-thickness skin grafts on the paraspinal skin of a Yorkshire pig observed with the oxygen-sensing paint-on bandage. Top row: regular photographs; middle row: emission at 700 nm - oxygen-dependent phosphorescence signals are overwhelmed by the skin autofluorescence background; bottom-row: percent oxygen consumption (%) maps obtained after eliminating autofluorescence - blue indicates higher oxygen consumption by tissues. Red indicates lower oxygen consumption by tissues. Arrows indicate tattoo marks dividing grafts and surrounding skin. Images shown for A) full-thickness graft immediately post-grafting; B) partial-thickness graft immediately post-grafting; C) full-thickness graft at 1-month graft assessment; D) partial-thickness graft at 1-month graft assessment.

3.6. Visualizing in vivo graft incorporation using the oxygen-sensing bandage in a porcine graft model

Skin transplants are commonly used in burn interventions, with full-thickness skin grafts providing the best functional and aesthetic outcomes in patients [36]. However, their application is limited as it is often difficult to obtain enough autologous full-thickness skin from a patient [38]. Thus, autologous partial-thickness skin grafts are frequently used because they can cover larger tissue areas while requiring less donor skin (especially when processed by a skin mesher) [39]. Partial-thickness grafts, however, lack significant dermal structures and require oxygenation through direct diffusion from the underlying wound bed. Therefore, it is important for physicians to monitor the oxygenation of partial-thickness grafts to ensure they are successfully integrated following the engrafting procedures.

The oxygen-sensing bandage was tested on an *in vivo* porcine graft model that simulates the reconstructive surgical procedures used in many burn interventions. Full-thickness skin grafts and partial-thickness skin grafts were applied to circular excisional wounds established on the paraspinal skin of a Yorkshire pig. Graft oxygenation was measured with the oxygen-

#217203 - $15.00 USD Received 22 Jul 2014; revised 5 Sep 2014; accepted 5 Sep 2014; published 1 Oct 2014

sensing bandage immediately post-grafting and during the 1-month follow-up assessment session. Full-thickness grafts containing all the layers of skin as well as their underlying supporting tissue, depicted in Fig. 1(E), demonstrated normal or slightly decreased oxygen consumption rate immediately after grafting, as shown in Fig. 6(A). On the other hand, partial-thickness graft, depicted in Fig. 1(F), were observed to have a much slower oxygen consumption rate, as can be seen in Fig. 6(B). The consumption rates for both the full- and partial-thickness grafts were found to have resumed to normal level after one month, showing that both grafts were successfully integrated (Figs. 6(C), and 6(D)).

4. Conclusions

A paint-on bandage was developed for the non-invasive, two-dimensional mapping of tissue oxygenation and oxygen consumption using a camera-based device. The bandage contains oxygen-sensing molecules whose phosphorescence emission intensity and lifetime values change in a pO_2-dependent fashion. The system was tested on an *in vivo* rat ischemic limb model, which demonstrated its ability to sense tissue ischemia. It was then used to monitor the progression of burns in both *ex vivo* and *in vivo* porcine burn models. Lastly, it was applied to an *in vivo* porcine graft model to monitor the integration of full-thickness and partial-thickness skin grafts.

By incorporating oxygen-sensing capabilities into wound dressing materials, the transparent paint-on bandage described in this work may be applied to provide long-term wound protection and continuous access to the status of skin and wound oxygenation. This system has the potential to improve the clinical care of chronic ischemic wounds, burns, skin grafts/flaps and other tissue injuries where tissue oxygenation plays an important role in the patient's prognosis. The bandage is composed of materials known to be biocompatible and/or materials already in clinical use, thereby potentially reducing the barrier to both in-human clinical trials and future clinical use. Additionally, the imaging device developed here is portable and stable, does not require bedside calibration, and can be easily engineered for bedside use. As a non-invasive, passive device for tissue oxygenation measurement of both intact and compromised skin, this technology has excellent translational potential. It will also facilitate the study of local regulation of skin oxygenation that may lead to a better understanding of a variety of skin conditions.

Acknowledgments

The authors would like to thank Joachim Pruessner (Api) for his help with diagram design and creation. This research is sponsored in part by the Air Force Office for Scientific Research, under grant number: FA9550-13-1-0068. The authors also gratefully acknowledge funding from the National Institute of Health, under grant number: 1 DP2 OD007096-1. Information on the New Innovator Award Program is at http://nihroadmap.nih.gov/newinnovator/.

#217203 - $15.00 USD Received 22 Jul 2014; revised 5 Sep 2014; accepted 5 Sep 2014; published 1 Oct 2014